Available online at www.sciencedirect.com
SCIENCE DIRECT®
Polymer 44 (2003) 3259–3267
polymer
www.elsevier.com/locate/polymer

Melting and crystallization behavior of poly(trimethylene 2,6-naphthalate)

Young Gyu Jeong[a], Won Ho Jo[a,*], Sang Cheol Lee[b]

[a]*Hyperstructured Organic Materials Research Center and School of Materials Science and Engineering, Seoul National University, Sun 56-1, Shinlim-Dong, Kwanak-ku, Seoul 151-742, South Korea*
[b]*School of Advanced Materials and Systems Engineering, Kumoh National University of Technology, Kumi 730-701, South Korea*

Received 5 November 2002; received in revised form 7 February 2003; accepted 24 March 2003

Abstract

The melting and crystallization behavior of poly(trimethylene 2,6-naphthalate) (PTN) are investigated by using the conventional DSC, the temperature-modulated DSC (TMDSC), wide angle X-ray diffraction (WAXD) and polarized light microscopy. It is observed that PTN has two polymorphs (α- and β-form) depending upon the crystallization temperature. The α-form crystals develop at the crystallization temperature below 140 °C while β-form crystals develop above 160 °C. Both α- and β-form crystals coexist in the samples crystallized isothermally at the temperature between 140 and 160 °C. When complex multiple melting peaks of PTN are analyzed using the conventional DSC, TMDSC and WAXD, it is found that those arise from the combined mechanism of the existence of different crystal structures, the dual lamellar population, and melting–recrystallization–remelting. The equilibrium melting temperatures of PTN α- and β-form crystals determined by the Hoffman–Weeks method are 197 and 223 °C, respectively. When the spherulitic growth kinetics is analyzed using the Lauritzen–Hoffmann theory of secondary crystallization, the transition temperature of melt crystallization between regime II and III for the β-form crystals is observed at 178 °C. Another transition is observed at 154 °C, where the crystal transformation from α- to β-form occurs.

Keywords: Poly(trimethylene 2,6-naphthalate); Melting behavior; Crystallization behavior

1. Introduction

Poly(trimethylene 2,6-naphthalate) (PTN) is a semicrystalline polymer whose preparation was first reported in 1969 [1]. As can be seen in Fig. 1, the chemical structure of PTN is equivalent to that of poly(trimethylene terephthalate) (PTT) except that a benzene ring in PTT is replaced by a naphthalene ring. Since 1,3-propanediol and 2,6-naphthalenedicarboxylic acid have been recently produced in large scale, it has been recognized that PTN has a high potential as an engineering plastic. Accordingly, several studies on polymerization kinetics, characterization, rheological, and thermal properties of PTN have been reported [2–6]. Nevertheless, studies on the crystal structure, crystallization and melting behavior of PTN have not been accomplished until recently. It has firstly been identified by ours that PTN exhibits two different crystal structures, i.e. α- and β-form depending upon crystallization temperature, as listed in Table 1 [7].

It is generally known that macroscopic properties of semicrystalline polymers are governed by their microscopic morphology, which in turn depends on their crystallization condition and on their thermal history. For this reason, the melting and crystallization behavior of semicrystalline polymers such as polyesters [8–17] and poly(ether ether ketone) (PEEK) [18–28] have been intensively studied. Particularly, the observation of multiple melting endotherms for these semicrystalline polymers during differential thermal analysis has attracted much interest. A variety of explanations for this phenomenon have been suggested, namely, (i) the existence of different crystal structures [29–32], (ii) the dual lamellar population model due to the primary and secondary crystallization [12,17,23,26–28], and (iii) the melting–recrystallization–remelting model [9,10,18–22,25].

A mechanism of multiple melting behavior due to the existence of different crystal structures has been proposed for syndiotactic polystyrene [29,30], isotactic polypropylene [31], and poly(vinylidene fluoride) [32]. In the dual lamellar population model, primary lamellar crystals are first formed comprising thicker crystalline lamellae, and

* Corresponding author. Tel.: +82-2-880-7192; fax: +82-2-885-1748.
E-mail address: whjpoly@plaza.snu.ac.kr (W.H. Jo).

0032-3861/03/$ - see front matter © 2003 Elsevier Science Ltd. All rights reserved.
doi:10.1016/S0032-3861(03)00270-2

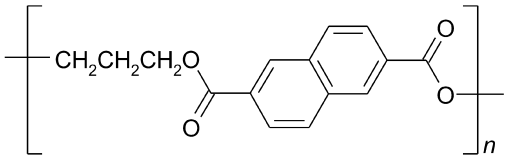

Fig. 1. Chemical structure of poly(trimethylene 2,6-naphthalate).

secondary lamellar crystals are then formed between the primary lamellar crystals [12,17,23,26–28]. In the melting–recrystallization–remelting model, the lamellar crystals present initially melt, the melted lamellar crystals undergo a continuous process of recrystallization yielding thicker lamellar crystals, and then the recrystallized crystals melt at higher temperatures [9,10,18–22,25]. It has been explained that the multiple melting behavior for condensation polymers such as PET, PEN and PEEK is a consequence of either dual lamellar population or melting–recrystallization–remelting. In some cases, it has been reported that the multiple melting behavior originates from the combined mechanism among them [29,30].

The purpose of this study is to elucidate the mechanism of the melting and crystallization behavior of PTN using the conventional DSC, the temperature-modulated DSC (TMDSC), wide angle X-ray diffraction (WAXD) and polarized light microscopy. In addition, the spherulitic crystallization kinetics of PTN is analyzed in terms of the transitions of crystallization by using the Lauritzen–Hoffman theory of secondary nucleation [33].

2. Experimental

2.1. Materials and sample preparation

PTN used in this study was synthesized by melt-condensation of 1,3-propandiol (PD) with dimethyl-2,6-naphthalate (DMN) using tetraisopropyl orthotitanate as a catalyst. Two-step polymerisation was performed on a laboratory-scale polymerisation reactor in the melt state. The first step was the transesterification reaction of DMN with PD, and the second was the polycondensation reaction.

Table 1
Crystallographic data for PTN

	α-form	β-form
Crystal system	Monoclinic	Triclinic
Unit cell parameters		
a (nm)	0.744	0.467
b (nm)	0.709	0.701
c (nm)	2.384	2.218
α (°)	90.0	100.8
β (°)	90.0	88.8
γ (°)	81.6	120.6
Repeating units/unit cell	4	2
Unit cell density (g/cm^3)	1.368	1.393
Unit cell volume (nm^3)	1.244	0.611

The transesterification reaction was carried out at 190 °C under nitrogen atmosphere, and the extent of reaction was monitored by measuring the amount of methanol evolved. The polycondensation was carried out at 260 °C under high-vacuum condition. At the end of the reaction, the product in the melt was quenched into water bath and followed by drying in a vacuum oven for several days. The intrinsic viscosity of PTN measured in a mixed solvent of phenol/1,1,2,2-tetrachloroethane (6/4, v/v) at 35 °C with an Ubbelohde capillary viscometer was 0.74 dl/g, indicating that the PTN samples synthesized have relatively high molecular weights enough to form in film.

To investigate the melting of PTN, isothermally melt-crystallized samples were prepared by heating the sample to 235 °C, holding for 3 min in order to melt crystals completely, rapidly cooling to the predetermined crystallization temperature (T_c), crystallizing at that temperature for several hours, and then quenching into room temperature.

2.2. Wide angle X-ray diffraction analysis

WAXD patterns of the PTN samples isothermally crystallized at various temperatures were obtained with a MAC Science M18XHF X-ray diffractometer using Ni-filtered Cu Kα radiation ($\lambda = 0.1541$ nm; 50 kV; 100 mA) at a scanning rate of 2°/min. The diffractometer was operated in the reflection mode and equipped with a $\theta/2\theta$ goniometer, a divergence slip (1.0°), a scattering slit (1.0°), and a receiving slit (0.30 mm). The X-ray measurements were performed at room temperature. The sample-to-detector distance or d-spacing was calibrated using Si powder ($2\theta = 28.44°$) as a standard. The X-ray crystallinity (x) for the PTN samples melt-crystallized isothermally at various temperatures was evaluated from the diffracted intensity data in the range of $2\theta = 5–50°$ using the relation, $x = A_{cr}/(A_{cr} + A_{am})$, where A_{cr} and A_{cr} denote the total crystalline and amorphous scattering, respectively, after correction of the Lorentz and polarization factors [34]. Amorphous contribution to the X-ray scattering was estimated from the WAXD pattern for the melt-quenched amorphous sample.

2.3. Melting behavior

The melting behavior of melt-crystallized sample was investigated by using the conventional DSC and TMDSC. A Perkin–Elmer DSC-7 equipped with an intercooler system was used as a conventional DSC. Relatively small sample size of 5 ± 0.3 mg was used to minimize the effect of thermal conductivity of samples. Unless otherwise specified, the heating and cooling rate were 20 and 10 °C/min, respectively. All DSC runs were carried out under nitrogen atmosphere to minimize the oxidative degradation. The TMDSC measurements were performed on a TA instruments 2920 MDSC equipped with a refrigerated cooling

system. Nitrogen gas was used as a purge gas and the flow rate was 35 ml/min. Standard modulation conditions used in our experiments were a period of 60 s, a heating rate of 2 °C/min, and an amplitude of 0.318 °C, as recommended in specifications of the manual of TA instruments, Inc [35]. The amplitude was selected for 'heating only' condition to separate the complex melting and crystallization transitions. The sample weight was controlled ca. 10 mg. Before all DSC experiments, the baseline was calibrated using empty crimped aluminum pans, and the melting temperature and the heat of fusion was calibrated using a high-purity indium standard (156.6 °C and 28.45 J/g). The peak temperature of melt-crystallized sample was taken as the melting or crystallization temperature.

2.4. Crystallization kinetics

Isothermal spherulitic growth rate of PTN was measured using a polarized light microscopy (Leica PX-3000) equipped with a Mettler hot stage (model FP-90) and a video recording system. Specimen was prepared by melting the PTN sample on a slide glass on a hot stage at 235 °C, pressing the melted sample with a piece of cover glass, and followed by maintaining for 3 min at this temperature to remove thermal history. The sample was then rapidly transferred onto the hot stage controlled to a predetermined crystallization temperature between 120 and 200 °C. The subsequent spherulitic growth was monitored between crossed polars, and recorded at an appropriate time interval by a video recorder mounted on the microscope. The radius of spherulite was measured directly from the video-recorded image. The spherulitic growth rate was determined from the slope of the radius of spherulite versus time plot. Three separate measurements at a given crystallization temperature are averaged for improving its statistics.

3. Results and discussion

3.1. Melting behavior of the melt-crystallized PTN by conventional DSC

When WAXD patterns of PTN melt-crystallized isothermally at various temperatures are examined, the patterns are classified into two groups, as shown in Fig. 2. The samples crystallized isothermally below 140 °C show one form of crystal, so-called α-form crystal, whereas the samples above 160 °C develop the other form of crystal, so-called β-form crystal. Both α- and β-form crystals coexist in the samples crystallized isothermally between 140 and 160 °C. As the crystallization temperature increases from 140 to 160 °C, the relative fraction of α-form crystal decreases.

Fig. 3 shows that PTN samples have one to five melting endotherms depending upon isothermal crystallization temperature. When the melting temperatures in Fig. 3 are

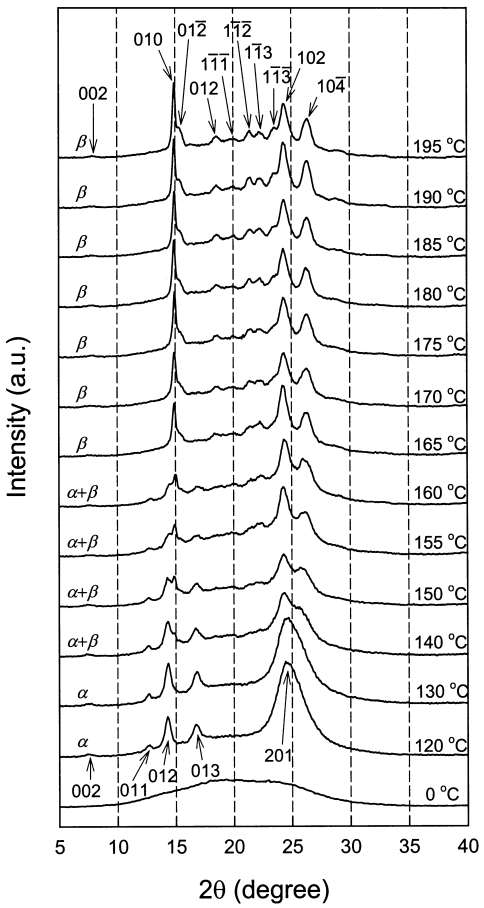

Fig. 2. X-ray diffraction patterns of the PTN samples isothermally melt-crystallized at various temperatures.

compared with WAXD patterns in Fig. 2, T_{m1} can be assigned to melting of the secondary α-form crystals, T_{m2} to melting of the secondary β-form crystals, T_{m3} to melting of the primary α-form crystals, T_{m4} to melting of the primary β-form crystals, and T_{m5} to melting of the recrystallized α- and/or β-form crystals. The primary α- or β-form crystals and the secondary α- or β-form crystals indicate lamellar crystals formed by the primary and secondary crystallization during isothermal crystallization, respectively. It should be noted that the PTN sample melt-crystallized isothermally at 140 °C has both α- and β-form crystals whereas the sample melt-crystallized isothermally at 170 °C has only β-form crystals, as can be seen in X-ray diffraction pattern of Fig. 2. In order to identify the origin of the respective melting peak, the samples melt-crystallized isothermally at 140 and 170 °C are heated at different heating rates. As can be seen in Fig. 4A, the melting temperatures (T_{m1} and T_{m2}) of the secondary α- and β-form crystals show broad bimodal melting, and the T_{m3} due to melting of primary α-form crystals becomes larger as the heating rate increases. Here it is noted that two separate melting peaks (T_{m1} and T_{m2}) in Fig. 4A due to the secondary α- and β-form crystals is a peculiar phenomenon and is firstly observed by ours. This observation leads us to

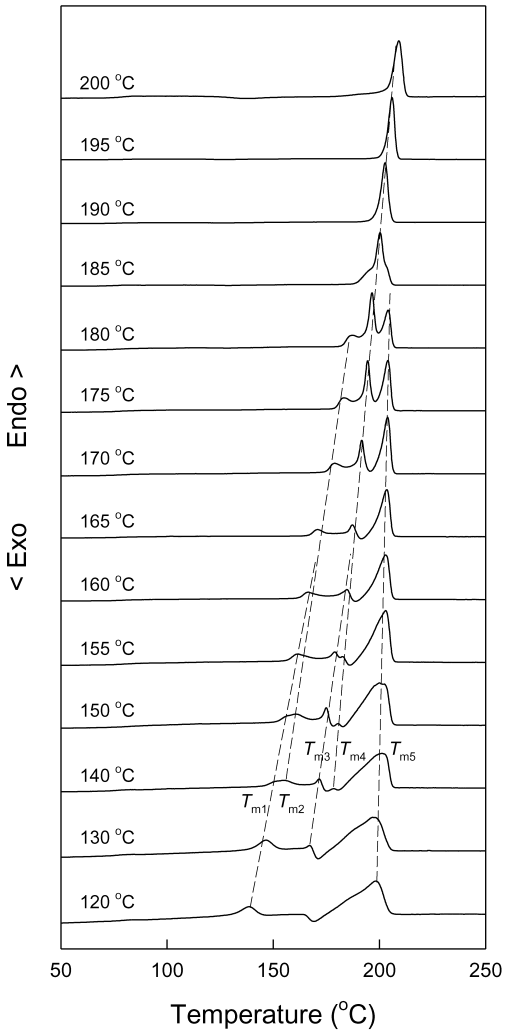

Fig. 3. Conventional DSC heating thermograms of the PTN samples isothermally melt-crystallized at various temperatures.

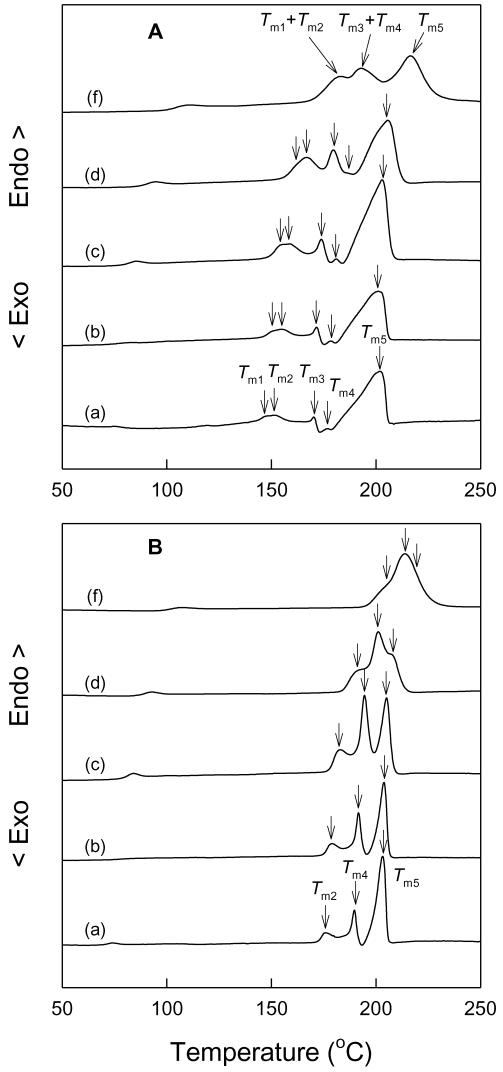

Fig. 4. Conventional DSC heating thermograms of the PTN samples isothermally melt-crystallized at the temperature of (A) 140 °C and (B) 170 °C at various heating rates: (a) 10 °C/min; (b) 20 °C/min; (c) 40 °C/min; (d) 80 °C/min; (e) 160 °C/min.

conclude that the crystal form of secondary lamellae crystals is strongly dependent upon the crystal form of primary lamellae crystals, when the secondary lamellae crystals are formed between primary lamellae crystals. The subsequent exothermic heat flow following T_{m3} results from recrystallization of the melted primary α-form crystals. This exothermic heat flow becomes diminished with increasing the heating rate, because the melted primary α-form crystals may not have enough time to recrystallize at fast heating rate. The melting peak (T_{m4}) of primary β-form crystals is clearly observed up to the heating rate of 40 °C/min. At heating rates faster than 40 °C/min, T_{m3} and T_{m4} (or T_{m1} and T_{m2}) become merged and finally indiscernible each other. Therefore, It is tentatively concluded from the above results that the multiple melting behavior of the sample melt-crystallized isothermally at 140 °C originates from the combined mechanism of the existence of different crystal structures, the dual lamellar population due to the primary and secondary crystallization, and the melting–recrystallization–remelting. This multiple melting behavior will be clearly analyzed using TMDSC in Section 3.2. When the PTN sample is melt-crystallized isothermally at 170 °C, the lowest endotherm (T_{m2}) in DSC thermograms is due to melting of the secondary β-form crystals, T_{m4} to melting of primary β-form crystals, and T_{m5} to melting of the recrystallized β-form crystals, as shown in Fig. 4B. As the heating rate is increased, the melting endotherm (T_{m5}) of recrystallized β-form crystals become smaller, while the melting endotherm (T_{m4}) of primary β-form crystals becomes larger. As a result, the multiple melting behavior of the samples melt-crystallized isothermally at 170 °C is originated from the combined mechanism of the dual lamellar population model and the melting–recrystallization–remelting model. Combining the results of WAXD patterns (Fig. 2) with the DSC thermograms (Fig. 3) leads us to conclude that only α-form crystals develop below 140 °C, only β-form crystals above 160 °C, and mixed crystals

of α- and β-form coexist in the sample melt-crystallized isothermally between 140 and 160 °C.

The equilibrium melting temperatures (T_m^0) of PTN α- and β-form crystals can be determined by using the Hoffman–Weeks plots as shown in Fig. 5. More specifically, the T_m^0 is obtained by extrapolating the plot of T_m versus T_c to the line $T_m = T_c$. The T_m^0's of PTN α- and β-form crystals are determined to be 197 and 223 °C, respectively.

3.2. Melting behavior of the melt-crystallized PTN by TMDSC

In order to understand more clearly the origin of complex melting behavior of the melt-crystallized PTN, we have used the TMDSC technique. The TMDSC as a new technique [36–39] has provided not only all information as does the conventional DSC, but also provided unique information not available from the conventional DSC. The TMDSC signal detects the melting of crystals present originally in the sample as an endothermic peak. Such information can be not obtained from the conventional DSC, because exothermic and endothermic events occur simultaneously on heating or cooling process in the conventional DSC. The TMDSC provides the total heat flow from the conventional DSC as well as the heat capacity-related reversible component of the heat flow. The difference between the total heat flow and the reversing heat flow is a non-reversing heat flow [36–39]. The reversing signal is effective for quantifying the glass transition and separates the glass transition completely from other non-reversing processes such as enthalpy relaxation and crystallization.

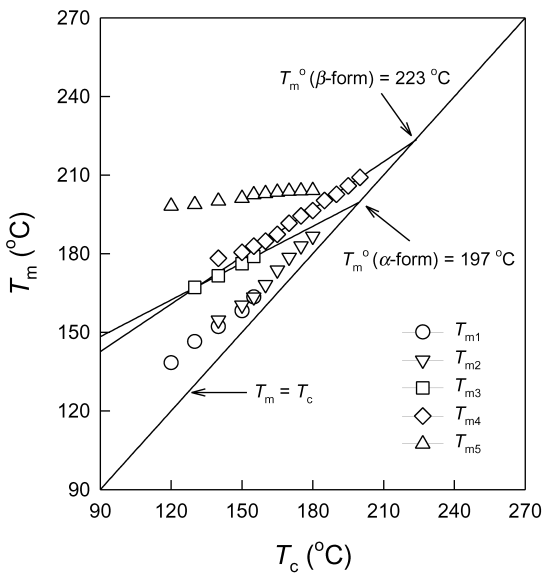

Fig. 5. Hoffman–Weeks plots for determining the equilibrium melting temperatures of PTN α- and β-form crystals from the conventional DSC data of the PTN samples isothermally melt-crystallized at various temperatures.

Exothermic events are completely absent from the reversing signals, enhancing the resolution of different thermal events. However, both the reversing and non-reversing signals can contain components of endothermic crystal melting, and their relative fractions depend on the types of crystals present and the experimental conditions. Recently, Sauer et al. [40] have successfully characterized the melting and recrystallization of polymers exhibiting multiple melting endotherms such as poly(ethylene 2,6-naphthalate) (PEN) and poly(oxy-1,4-phenyeneoxy-1,4-phenylenecarbonyl-1,4-phenylene) (PEEK) using both the conventional DSC and TMDSC, where the TMDSC signal detects the melting of crystals present originally in the sample as endothermic peaks. They discussed in detail the reason why the endothermic peaks of primary and secondary crystals appear separately in the reversing and non-reversing signals in TMDSC thermograms, respectively, and the reason why the exothermic peak of crystallization appears in the reversing signal.

The TMDSC thermograms for the PTN sample melt-crystallized isothermally at 120 °C, which has only α-form crystals, are shown in Fig. 6A. A melting endothermic peak (T_{m1}) due to melting of the secondary α-form crystals is observed at ca. 133 °C in total and non-reversing signals, and the melting endotherm (T_{m3}) of primary α-form crystals present originally in the sample is observed at ca. 170 °C in reversing signal. Particularly, the exothermic recrystallization starts just after the endothermic melting of primary

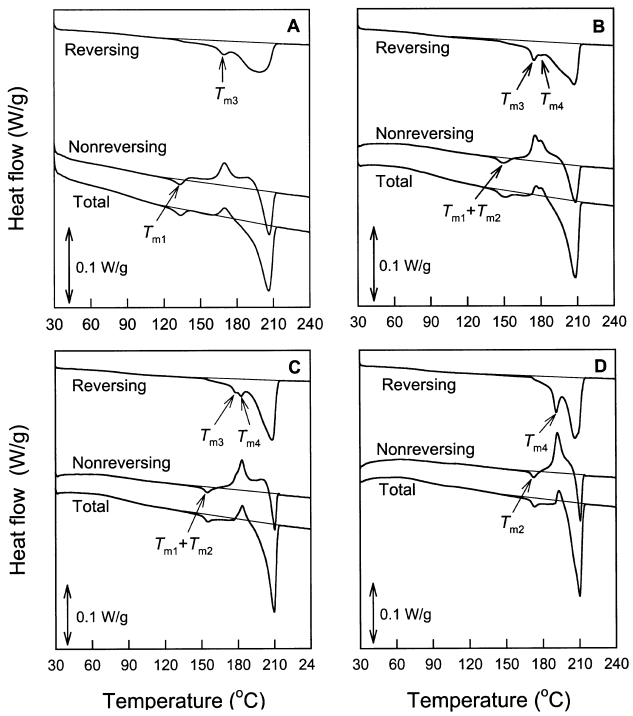

Fig. 6. TMDSC heating thermograms for the PTN sample isothermally melt-crystallized at various temperatures: (A) 120 °C; (B) 140 °C; (C) 150 °C; (D) 170 °C.

α-form crystals, as can be seen in non-reversing signal of Fig. 6A. Here, it is assumed that the recrystallization of primary α-form crystals is accompanied with the crystal transformation from α- to β-form crystals. This assumption is supported from the facts that a broad melting endotherm of recrystallized crystals is observed in reversing signal and that the melting point of the recrystallized crystals is observed in total heat flow signal at 206 °C, which is higher than T_m^0 (= 197 °C) of α-form crystals and lower than that of β-form crystals.

As noted in Section 3.1, the PTN samples melt-crystallized isothermally between 140 and 160 °C have both α- and β-form crystals. The TMDSC thermograms of the PTN sample melt-crystallized isothermally at 140 and 150 °C are shown in Fig. 6B and C, respectively, where the total heat flow signal is somewhat different from the conventional DSC thermogram in Fig. 3. This is because the melting and recrystallization in the conventional DSC strongly depend upon the heating rate. As can be seen in Fig. 6B, a broad endothermic peak (T_{m1} and T_{m2}) is observed around 150 °C due to melting of the secondary α- and β-form crystals in non-reversing and total signals. Two separate endothermic peaks due to the respective melting (T_{m3} and T_{m4}) of primary α- and β-form crystals formed during isothermal crystallization are detected in reversing signal while two separate exothermic peaks due to recrystallization from the melted primary α- and β-form crystals are observed in non-reversing signal. The observation of double endothermic and exothermic peaks lead us to conclude that the melting and recrystallization process of primary α- or β-form crystals occur independently. Here, the possibility to transform from α- to β-form may not be excluded during the process of crystal melting-recrystallization as mentioned above.

When the PTN sample is isothermally melt-crystallized at 170 °C, the sample has only β-form crystals, as shown in Fig. 6D. A melting endothermic peak (T_{m2}) due to melting of the secondary β-form crystals is observed at ca. 169 °C in non-reversing signal, and the melting endothermic peak (T_{m4}) of primary β-form crystals present originally in the sample is observed at ca. 190 °C in reversing signal. The exothermic recrystallization starts just after the endothermic melting of primary β-form crystals, as can be seen in non-reversing signal of Fig. 6D. Therefore, it is concluded that the multiple melting behavior of the PTN sample melt-crystallized isothermally at 170 °C originates from the combined mechanism of the dual lamellar population and melting–recrystallization–remelting.

3.3. Isothermal crystallization behavior of PTN

Figs. 7–9 show the polarized light micrographs of PTN crystallized isothermally at 140, 160, and 170 °C, respectively. For all cases, the crystals grow spherically, and these spherulites exhibits a typical negative birefringence when the samples are observed under polarized light microscope

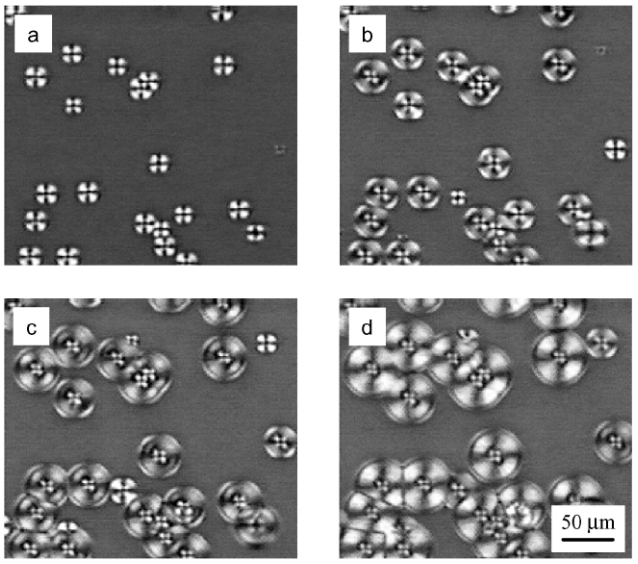

Fig. 7. Polarized light micrographs of PTN isothermally melt-crystallized at 140 °C: (a) 5 min; (b) 10 min; (c) 15 min; (d) 20 min.

with a gypsum plate, i.e. the first and third quadrants of spherulite appear yellow but the second and fourth quadrants appear blue [41]. In addition to this usual observation for polymers, distinct concentric rings can be seen when the samples are crystallized at higher crystallization temperature above 160 °C, as shown in Figs. 8 and 9. This ringed image is similar to the banded spherulite morphology. Although it is generally accepted that the formation of banded spherulites is attributed to the lamellar twisting along the radius of spherulite, no concrete agreement is found on the origin of the lamellar torsion [42–45]. Although it is difficult to clarify the relationship between banded spherulites and polymorphism, the banded

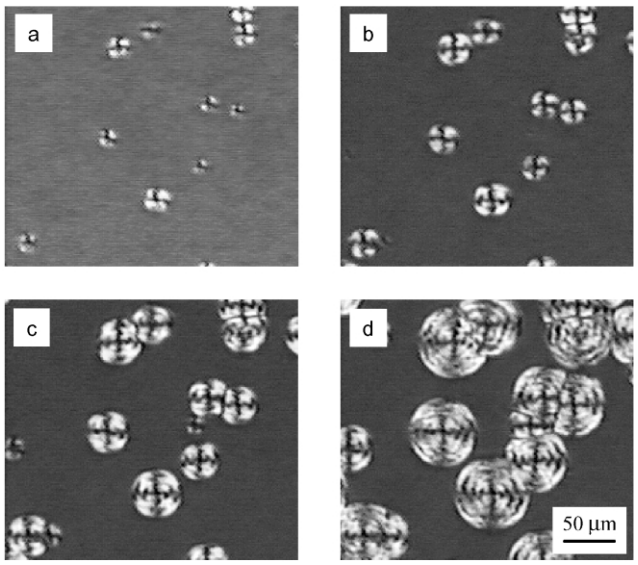

Fig. 8. Polarized light micrographs of PTN isothermally melt-crystallized at 160 °C: (a) 4 min; (b) 8 min; (c) 12 min; (d) 16 min.

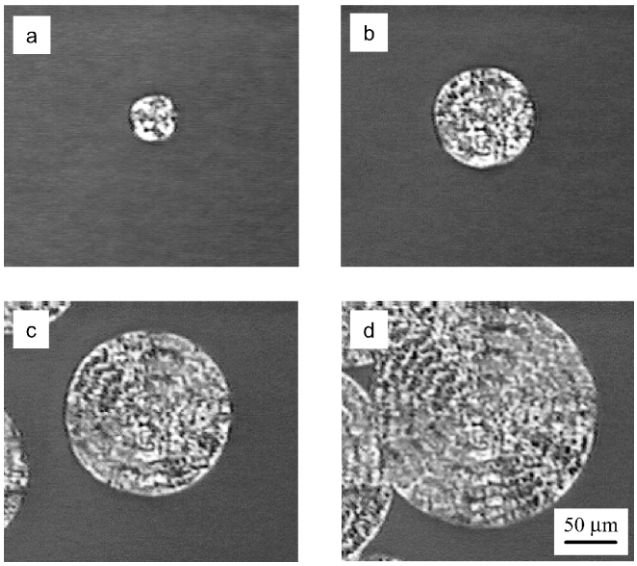

Fig. 9. Polarized light micrographs of PTN isothermally melt-crystallized at 170 °C: (a) 10 min; (b) 25 min; (c) 40 min; (d) 55 min.

extinction of spherulites becomes clearer and the band spacing increases with increasing the crystallization temperature.

When Figs.7–9 are compared with each other, it reveals that the dimension of the spherulites is very sensitive to the crystallization temperature and time. When the radii of spherulites measured from a series of video images taken at successive intervals are plotted as a function of time for various crystallization temperatures, the spherulitic growth rate is determined from the slope of a linear least-squares fit of the plot, as shown in Fig. 10. The linearity of the plot means that the radius of spherulite is increased linearly with time until the spherulites impinge on each other. When the spherulitic growth rate (G) is plotted against crystallization

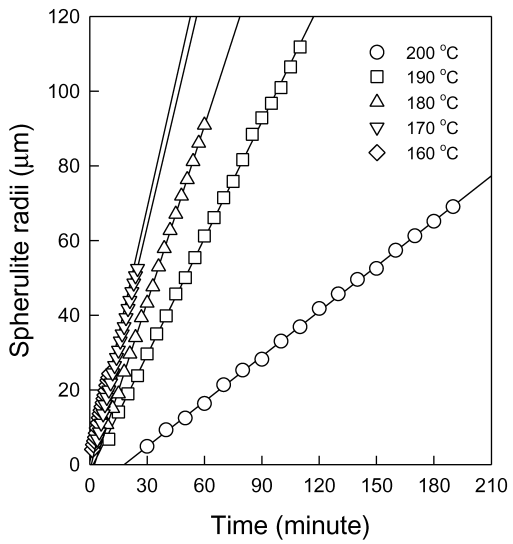

Fig. 10. Plots of radius of spherulite versus time when the sample is isothermally crystallized at different temperatures.

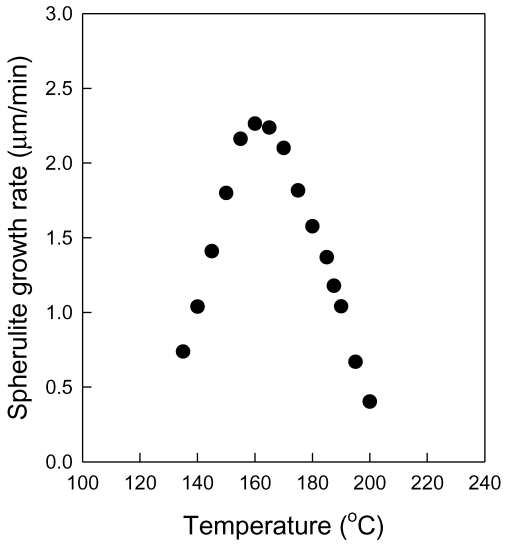

Fig. 11. Plot of spherulitic growth rate of PTN versus isothermal melt-crystallization temperature. The spherulitic growth rate is determined from the slope of the plot of spherulite radius versus time in Fig. 10.

temperature, the maximum growth rate is observed at the crystallization temperature of ca. 160 °C, as shown in Fig. 11.

The spherulitic growth rate of PTN is analyzed using the secondary crystallization theory proposed by Lauritzen and Hoffman as following [33]:

$$G = G_o \exp\left(\frac{-U^*}{R(T_c - T_\infty)}\right)\exp\left(\frac{-K_g}{T_c \Delta T f}\right) \quad (1)$$

where G_o is a pre-exponential factor which is not strongly dependent on temperature, U^* is the activation energy for the transportation of segments of molecules across the melt/solid surface boundary and is usually given by a universal value of 1500 cal/mol, R is the gas constant, $T_\infty (= T_g - 30\,°C)$ is the temperature below which all viscous flow stops, ΔT is the degree of supercooling defined by $T_m^0 - T_c$, $f (= 2T_c/(T_m^0 + T_c))$ is a correction factor which accounts for the variation in the heat of fusion of perfect crystal with temperature, and K_g is the nucleation exponent and is defined as

$$K_g = \frac{\xi b_o \sigma \sigma_e T_m^0}{k \Delta H_f^0} \quad (2)$$

where ξ equals 2 for regime II and 4 for regimes I and III, b_o denotes the crystal layer thickness along the growth direction, σ and σ_e are the lateral and fold surface free energy, respectively, T_m^0 is the equilibrium melting temperature, k is the Boltzmann's constant, and ΔH_f^0 is the equilibrium heat of fusion per unit volume. It is often convenient to rearrange Eq. (1) as the following equation:

$$\ln G + \frac{U^*}{R(T_c - T_\infty)} = \ln G_o - \frac{K_g}{T_c \Delta T f} \quad (3)$$

When the value of the left-hand side of Eq. (3) is plotted

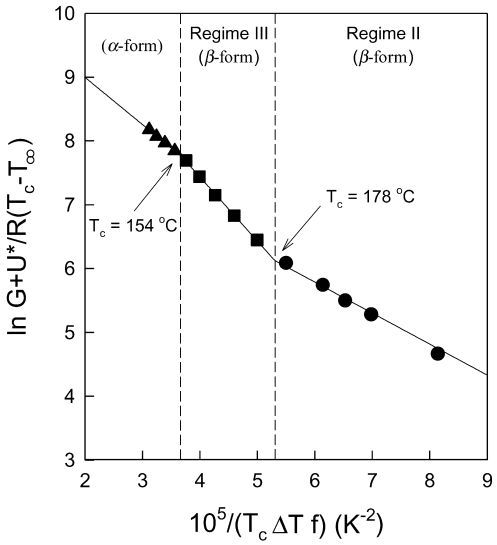

Fig. 12. Analysis of the spherulitic growth rate of PTN using the secondary nucleation theory proposed by Lauritzen and Hoffman.

against $1/(T_c\Delta Tf)$, as shown in Fig. 12, the nucleation exponent (K_g) is determined from the slope of the plot. Fig. 12 shows that a transition between regime II and III for the β-form crystals is found in the vicinity of 178 °C ($\Delta T \cong 47\,^{\circ}C$). It appears reasonable to fit the experimental data with two straight lines, and from each slope one obtains the $K_g(\mathrm{II}) = 0.49 \times 10^5$ and $K_g(\mathrm{III}) = 1.00 \times 10^5$. The ratio of the value of K_g (III) to the value of K_g (II) is 2.04, which is very close to 2.0 as predicted by the Lauritzen–Hoffman theory.

The value of K_g can be used to calculate σ_e of the PTN β-form crystal from Eq. (2). Using the layer thickness $b_o = 0.7014$ nm, $T_m^0 = 223$ °C and $\Delta H_f^0 = 141.75$ J/cm^3 (= 101.76 J/g × 1.393 g/cm^3), the value of $\sigma\sigma_e$ is estimated to be 136.50 erg^2/cm^4. The value of $\Delta H_f^0 = 101.76 \pm 5.52$ J/g is an average value evaluated from the crystallinity by X-ray diffraction in Fig. 2 and the heat of fusion by TMDSC for the PTN samples crystallized at various temperatures between 165 and 200 °C. The lateral surface-free energy (σ) may be estimated by the Thomas–Stavely relationship [46]

$$\sigma = \alpha\Delta H_f^0 (a_o b_o)^{1/2} \tag{4}$$

where a_o is the molecular width, and α is an empirical constant and usually assumed to be ca. 0.1. Taking $\alpha = 0.1$, σ can be estimated to be 8.11 erg/cm^2 from Eq. (4), and finally the fold surface free energy $\sigma_e = 16.83$ erg/cm^2.

Another important feature from Fig. 12 is that there exists a transition at 154 °C. This is probably due to the crystal transformation between PTN α- and β-forms. The PTN α-form crystal develops below 154 °C, whereas the PTN β-form crystal begins to develop above 154 °C. This crystal transformation temperature is well consistent with the results of X-ray diffraction, conventional DSC and TMDSC.

4. Conclusions

The melting and crystallization behavior of poly(trimethylene 2,6-naphthalate) (PTN) are systematically investigated using various instruments. It is observed that PTN has two polymorphs (α- and β-form) depending upon the crystallization temperature. The α-form crystals develop below 140 °C, whereas β-form crystals develop at the crystallization temperature above 160 °C. Both α- and β-form crystals coexist in the samples crystallized isothermally at the temperature between 140 and 160 °C. When complex multiple melting peaks of PTN are analyzed using the conventional DSC, TMDSC and WAXD, it is found that the multiple melting peaks arise from the combined mechanism of the existence of different crystal structures of α- and β-form, the dual lamellar population as the result of primary and secondary crystallization, and melting–recrystallization–remelting. The use of TMDSC allows us to successfully assign the exact melting temperatures of the primary α- and β-form crystals of the PTN samples melt-crystallized isothermally at various temperatures. The equilibrium melting temperatures of PTN α- and β-form crystals determined by the Hoffman–Weeks method are found to be 197 and 223 °C, respectively. When the morphology and spherulitic growth rate of PTN was examined by polarized light microscopy, it was found that the PTN samples crystallized isothermally at high temperatures show negative spherulites and banded spherulite morphology. The kinetics of spherulitic growth is analyzed using the Lauritzen–Hoffmann theory for the secondary nucleation, from which kinetic parameters are obtained. Isothermal crystallization from the melt is found to occur within the regime II and III for the PTN β-form crystal. The transition temperature from the regime II to III is determined to be 178 °C. Another transition is observed at 154 °C, which arises from the change of crystallization mechanism of PTN due to the crystal transformation from α- to β-form crystal.

Acknowledgements

The authors thank the Korea Science and Engineering Foundation (KOSEF) for financial support through the Hyperstructured Organic Materials Research Center (HOMRC).

References

[1] Duling IN, Chester W. US Patent 3,436,376; 1969.
[2] Tsai RS, Lee YD. J Polym Res 1998;5(2):77.
[3] Hwang SK, Yeh C, Chen LS, Way TF, Tsay LM, Liu KK, Chen LT. Polym Prepr 1999;40:611.
[4] Stier U, Gahr F, Oppermann W. J Appl Polym Sci 2001;80:2039.
[5] Stier U, Oppermann W. J Polym Sci Part B: Polym Phys 2001;39:620.
[6] Stier U, Schawaller D, Oppermann W. Polymer 2001;42:8753.

[7] Jeong YG, Jo WH, Lee SC. Proc Kor Text Conf 1999;32(2):307.
[8] Holdsworth PJ, Turner-Jones A. Polymer 1971;12:195.
[9] Groeninckx G, Reynaers H. J Polym Sci Polym Phys Ed 1980;18: 1325.
[10] Qiu G, Tang Z, Huang N, Gerking L. J Appl Polym Sci 1998;69:729.
[11] Wang ZG, Hsiao BS, Fu BX, Liu L, Yeh F, Sauer BB, Chang H, Schultz JM. Polymer 2000;41:1791.
[12] Hsiao BS, Wang ZG, Yeh F, Gao Y, Sheth KC. Polymer 1999;40: 3515.
[13] Cheng SZD, Wunderlich B. Macromolecules 1988;21:789.
[14] Buchner S, Wiswe D, Zachmann HG. Polymer 1989;30:480.
[15] Okamoto M, Kubo H, Kotaka T. Macromolecules 1998;31:4223.
[16] Lee SW, Cakmak M. J Macromol Sci Phys 1998;B37:501.
[17] Denchev Z, Nogales A, Ezquerra TA, Fernandes-Nascimento J, Balta-Calleja FJ. J Polym Sci Polym Phys Ed 2000;38:1167.
[18] Blundell DJ, Osborn BN. Polymer 1983;24:953.
[19] Blundell DJ. Polymer 1987;28:2248.
[20] Lee Y, Porter RS. Macromolecules 1987;20:336.
[21] Lee Y, Porter RS, Lin JS. Macromolecules 1989;22:1756.
[22] Jonas A, Legas R. Macromolecules 1993;26:813.
[23] Kruger KN, Zachmann HG. Macromolecules 1993;26:5202.
[24] Hsiao BS, Sauer BB, Verma RK, Zachmann HG, Seifert S, Chu B, Harrey P. Macromolecules 1995;28:6931.
[25] Jonas AM, Russell TP, Yoon DY. Macromolecules 1995;28:8491.
[26] Verma RK, Hsiao BS. Trends Polym Sci 1996;4:312.
[27] Verma RK, Velikov V, Karder RG, Marand H, Chu B, Hsiao BS. Polymer 1996;37:5357.
[28] Verma RK, Marand H, Hsiao B. Macromolecules 1996;29:7767.
[29] Sun YS, Woo EM. Macromolecules 1999;32:7836.
[30] Lin RH, Woo EM. Polymer 2000;41:121.
[31] Samuels RJ. J Polym Sci: Polym Phys Ed 1975;13:1417.
[32] Prest Jr WM, Luca DJ. J Appl Phys 1975;46:4136.
[33] Hoffman JD, Davis GT, Lauritzen JI. In: Hannay HB, editor. Treatise on solid state chemistry, vol. 3. New York: Plenum; 1975. Chapter 7.
[34] Bodor G. Structural investigation of polymers. New York: Ellis Horwood; 1991. pp. 305.
[35] Manual for DSC 2920 of TA Instruments, Inc. 1998, pC-75.
[36] Reading M. Trends Polym Sci 1993;8:248.
[37] Reading M, Elliot D, Hill VL. J Thermal Anal 1993;40:949.
[38] Okazaki I, Wunderlich B. Macromol Rapid Commun 1997;18:313.
[39] Okazaki I, Wunderlich B. Macromolecules 1997;30:1758.
[40] Sauer BB, Kampert WG, Neal Blanchard E, Threefoot SA, Hsiao BS. Polymer 2000;41:1099.
[41] Meeten GH. Optical properties of polymers. London: Elsevier Applied Science Publishers; 1986. p. 186.
[42] Keller A. J Polym Sci 1959;39:151.
[43] Hoffman JD, Lauritzen JI. J Res Natl Bur Stand 1961;65A:297.
[44] Keith HD, Padden FJ. Polymer 1984;25:28.
[45] Keith HD, Padden FJ, Lotz B, Wittmann JC. Macromolecules 1989; 22:2230.
[46] Thomas DG, Stavely LAK. J Chem Soc 1952;4569.